JGR Solid Earth

RESEARCH ARTICLE
10.1029/2019JB017679

On the Role of Stern- and Diffuse-Layer Polarization Mechanisms in Porous Media

Matthias Bücker[1,2,3], **Adrián Flores Orozco**[2], **Sabine Undorf**[3,4], **and Andreas Kemna**[3]

[1]Institute for Geophysics and extraterrestrial Physics, TU Braunschweig, Braunschweig, Germany, [2]Department of Geodesy and Geoinformation, Research Group Geophysics, TU Wien, Vienna, Austria, [3]Institute of Geosciences, Geophysics Section, Rheinische Friedrich-Wilhelms-Universität Bonn, Bonn, Germany, [4]School of GeoSciences, University of Edinburgh, Edinburgh, UK

Key Points:
- We investigate Maxwell-Wagner, Stern-layer and diffuse-layer, and membrane polarization in porous media in a generalized mathematical framework
- Numerical and analytical solutions are mutually verified, and existing analytical models of the four mechanisms are improved
- Low-frequency Stern-layer polarization is stronger than diffuse-layer polarization if the electrical double layer is discontinuous, only

Correspondence to:
M. Bücker,
m.buecker@tu-bs.de

Citation:
Bücker, M., Flores Orozco, A., Undorf, S., & Kemna, A. (2019). On the role of Stern- and diffuse-layer polarization mechanisms in porous media. *Journal of Geophysical Research: Solid Earth*, *124*, 5656–5677. https://doi.org/10.1029/2019JB017679

Received 12 MAR 2019
Accepted 24 MAY 2019
Accepted article online 31 MAY 2019
Published online 26 JUN 2019

Abstract Water-saturated porous media exhibit a low-frequency (<1 MHz) dispersion of the electrical conductivity caused by the polarization of the electrical double layer (EDL) coating the charged solid-liquid interface. We develop a mathematical framework describing the polarization caused by field-induced perturbations of the ion densities in the Stern and the diffuse layer of the EDL for two different geometrical configurations of solid and liquid phase. For spherical grains immersed in an electrolyte we derive an improved analytical description by combining suitable models for diffuse- and Stern-layer polarization. The selected models differ from those usually used in geophysical literature and improve the agreement with the corresponding finite-element solution significantly. We then employ the validated finite-element model to examine the EDL in a pore-constriction geometry, which is often used to study membrane polarization. Here, a suitable analytical model can only be set up for a pure diffuse-layer polarization. The results for the coupled Stern- and diffuse-layer polarization in both geometries indicate that (1) the polarization of the Stern layer is much stronger than the polarization of the diffuse layer as long as the EDL is not connected at the system scale; (2) this dominance of the Stern-layer polarization can be observed in both geometries, but (3) the contribution of the diffuse layer increases with increasing compaction as represented by the pore-constriction geometry; and (4) the contributions of both parts of the EDL reach similar levels, when the EDLs on different surfaces are interconnected at the system scale.

1. Introduction

Complex-conductivity measurements assess the frequency-dependent electrical conduction and polarization properties of soil and subsurface materials. Because macroscopic measurements are correlated to pore and/or grain geometry, electrochemical characteristics of the solid-liquid interface, and of the pore-filling electrolyte, the method has a huge potential for novel hydrogeophysical (e.g., Börner et al., 1996; Hördt et al., 2009) and biogeophysical (e.g., Atekwana & Slater, 2009; Flores Orozco et al., 2011; Wainwright et al., 2015) applications. Although empirical relations based on these correlations are increasingly used in near-surface studies, there is no widely accepted model linking macroscopic polarization effects to microscopic properties (e.g., Kemna et al., 2012). In absence of conductive minerals, four mechanisms contribute to the low-frequency (<1 MHz) dispersion of complex conductivity, all of which are sensitive to the polarization of different parts of the electrical double layer (EDL) at the solid-liquid interface (e.g., Lesmes & Morgan, 2001): (1) Maxwell-Wagner polarization, (2) polarization of the Stern layer, (3) polarization of the diffuse layer, and (4) membrane polarization.

Maxwell (1892) and Wagner (1914) studied interfacial polarization in heterogeneous media consisting of two or more phases of different electrical conductivity and/or dielectric constant: unequal conduction and displacement current densities in the different phases are balanced by an accumulation of charge along the geometrical boundaries. O'Konski (1960) extended the Maxwell-Wagner theory to include the polarization of charges bound to the surface of charged particles. Later, Garcia et al. (1985) treated the case of uncharged dielectric particles in electrolyte solution. In contrast to earlier theories, which assume homogeneous conductivities in both phases resulting in true surface charge distributions, their treatment accounts for local field-induced concentration variations in the electrolyte and thus volume charge of finite extension. The characteristic time scales of the different types of Maxwell-Wagner polarization are short, such that this relaxation usually occurs at the high-frequency limit (kHz) of the complex-conductivity response (e.g., Leroy et al., 2008; Lesmes & Morgan, 2001).

A first theory describing the polarization of the Stern layer was presented by Schwarz (1962) and improved by Schurr (1964). Schwarz' theory accounts for the diffusion-controlled polarization of the Stern layer of bound counterions. Schurr combined this model with the one by O'Konski to include the effect of surface conductivity due to the diffuse layer. Because the contribution of the diffuse layer is frequency independent in this model, the dispersion of the complex conductivity is attributed to Stern-layer polarization, and the diffuse layer only results in a uniform increase of the real part of the conductivity. Later, Schurr's model provided the basis for the treatment by Leroy et al. (2008), which includes a detailed electrochemical model to quantify the partition of charges into Stern and diffuse layer (see, e.g., Revil & Glover, 1997, 1998) and also accounts for a grain-size distribution. This model successfully predicted the response of glass beads (Leroy et al., 2008) and was extended to sand-oil-water mixtures later (Schmutz et al., 2010).

The polarization of the diffuse layer has been studied by Dukhin and Shilov (1974), who developed a theory for the ion fluxes through thin diffuse layers, which induce concentration variations in the diffuse layer and the adjacent electrolyte. This concentration-polarization mechanism has also been treated analytically by Fixman (1980), Chew and Sen (1982a), and Hinch et al. (1984) among others. A numerical solution removing many of the limitations of the analytical approaches—for example, the assumption of a thin diffuse layer compared to the particle radius, a sufficiently small surface potential, and a monovalent symmetric electrolyte—was presented by DeLacey and White (1981). Later, Shilov et al. (2001) included the effect of Maxwell-Wagner polarization into the classical Dukhin-Shilov theory yielding a good agreement with the numerical model by DeLacey and White (1981).

Different attempts have been made to determine the relative importance of Stern- and diffuse-layer polarization and to develop combined models. Lyklema et al. (1983) generalized the Schwarz-Schurr model by including the coupling of charges in the Stern layer to those in the diffuse layer, which mainly results in a decrease of the relaxation time scale. Leroy et al. (2017) applied this approach to model the polarization response of calcite precipitations on glass beads. de Lima and Sharma (1992) analyzed the models by Schwarz, Schurr, and Fixman separately in order to assess their relative contribution to the overall polarization response. By superposing the individual responses, Lesmes and Morgan (2001) developed a combined model considering all three polarization mechanisms, that is, Stern-/diffuse-layer and Maxwell-Wagner polarization. The authors also included a volume-averaging approach to study water-particle mixtures characterized by a grain-size distribution. Based on the work of Kijlstra et al. (1992), Shilov et al. (2001) modified the Dukhin-Shilov theory to account for the contribution of the Stern layer to surface conductivity.

Most theories describing the first three polarization mechanisms rest on the analytical solution of the underlying system of partial differential equations (PDEs) around one isolated spherical particle. The induced dipole moment of the polarized particle obtained from such treatment can then be used to derive the effective conductivity (or the effective dielectric constant) of ensembles of more than one particle. The effective medium theory provides mixing laws for dilute suspensions (e.g., Maxwell, 1892; Wagner, 1914) or mixtures with higher particle concentrations (e.g., Bruggeman, 1935; Hanai, 1960).

Membrane polarization is generally studied on pore networks with different levels of complexity. Marshall and Madden (1959) developed the first model for a sequence of two types of one-dimensional pores or zones. The membrane effect is introduced by assuming different mobilities for cations and anions in the "active" zone. While these authors do not further specify the origin of mobility variations, later developments related ion selectivity to the unequal contributions of cations and anions to the surface conductivity at the pore wall (Buchheim & Irmer, 1979; Fridrikhsberg & Sidorova, 1961; Titov et al., 2002, 2004). Blaschek and Hördt (2009) carried out numerical simulations on one- and two-dimensional pore networks, where the ion-selective behavior of narrow pores is still parameterized in terms of ion mobilities, which are constant over the pore cross section. Volkmann and Klitzsch (2010) improved this approach and limited the ion selectivity—expressed in terms of unequal effective ion mobilities—to a thin layer covering the pore walls.

Bücker and Hördt (2013a) proposed an analytical model, which allows to explicitly include pore radii and surface conductivity due to Stern and diffuse layer into the one-dimensional impedance model by Marshall and Madden. This model has later been extended to model the effect of temperature, fluid salinity, pH, and immiscible hydrocarbon contaminants on the polarization response (Bairlein et al., 2016; Bücker et al., 2017; Hördt et al., 2016). Based on the same model, Stebner et al. (2017) used impedance networks to model the membrane polarization of porous media. Because the model by Bücker and Hördt typically requires large

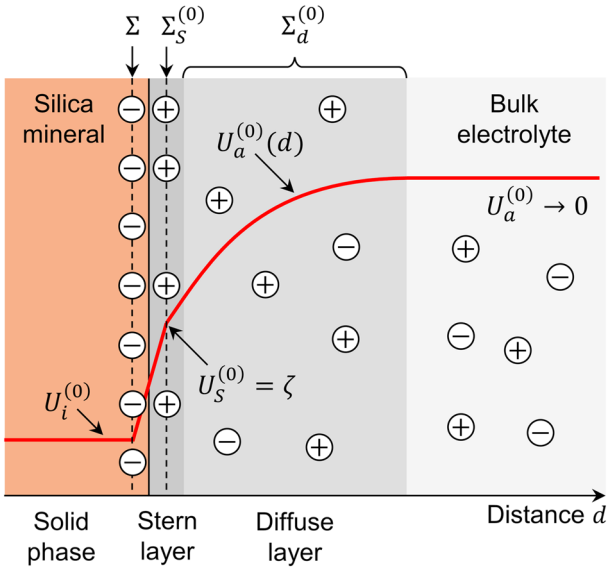

Figure 1. Simplified model of the equilibrium electrical double layer (EDL) at the charged silica surface. Due to the deprotonation of silanol surface sites, the mineral surface acquires the surface charge Σ. In the electrolyte, this usually negative charge is screened by an equal number of the positive charges distributed over the Stern layer ($\Sigma_S^{(0)}$) and the diffuse layer ($\Sigma_D^{(0)}$). The red line sketches the spatial variation of the electrical potential $U^{(0)}$ across the different parts of the electrical double layer.

aspect ratios, length of a pore divided by its diameter, to produce measurable polarization magnitudes, Hördt et al. (2017) further investigated into the geometrical constraints of this membrane-polarization model.

Besides geometrical constraints, the simplified consideration of the Stern layer is a major limitation of the existing theoretical treatment of membrane polarization. While combined treatments of Stern-layer, diffuse-layer, and Maxwell-Wagner polarization mechanisms exist for grain-based models, the coupling between these three mechanisms is often largely simplified in pore-constriction models. Irrespective from the model geometry, the complexity of the equations for the fully coupled system describing all three mechanisms puts a challenge on analytical solutions, which therefore all suffer from strong simplifications or only treat limiting cases.

The present paper addresses the repeatedly stated need for "a mechanistic approach and […] general framework in which all these mechanisms are explained and quantified in their relative importance" (Kemna et al., 2012). In the theory section, we compile the mathematical descriptions of all relevant physical processes and provide a mathematical framework, which allows modeling the fully coupled interplay of Stern- and diffuse-layer polarization on arbitrary geometries. Subsequently, we derive an improved analytical approximation for the polarization of a single grain, which matches the results obtained from numerically solving the equations of the generalized mathematical framework. The validated numerical model is then applied to the pore-constriction geometry. Based on the comparison of numerical and analytical results, we improve the membrane-polarization model by Bücker and Hördt (2013a) and for the first time study the fully coupled Stern- and diffuse-layer polarization in a pore-constriction geometry.

2. Theory

2.1. EDL Model

Most solid surfaces in contact with aqueous solutions are charged. We will consider silica surfaces in contact with a monovalent electrolyte, such as NaCl, where the deprotonation of silanol surface sites produces a negative surface-charge density Σ over a wide pH range (e.g., Leroy et al., 2008; Somasundaran, 2006). In the electrolyte next to the silica surface, the electric field of Σ attracts counterions (cations, if $\Sigma < 0$) and repels coions (here anions) giving rise to the development of two layers: The inner layer—also known as Stern or Helmholtz layer—consists of counterions adsorbed to the silica surface. The outer layer—also known as diffuse or Gouy-Chapman layer—is mainly populated by counterions and a minor fraction of coions both obeying Poisson-Boltzmann statistics.

We adopt the simplified model displayed in Figure 1. The Stern layer is treated as an infinitely thin layer of counterions (e.g., Leroy et al., 2008; Schwarz, 1962; Schurr, 1964) and is characterized by the uniform surface charge density $|\Sigma_S^{(0)}| < |\Sigma|$ (the superscript (0) indicates quantities in the equilibrium state, that is, without external excitation), which partly shields the electric field of Σ. Furthermore, we assume that charges in the Stern layer can only move along the surface, which reflects a strong binding of counter-ions to the surface.

The movement of the ions in the diffuse layer is not restricted to the surface; that is, these ions can move in all directions. As a result of an equilibrium between simultaneously acting electrostatic forces and thermal fluctuations, counterion excess and coion deficit concentrations smoothly decay with the distance d from the surface. At a far distance from the surface, both ion concentrations approach their values in the bulk electrolyte. Together with $\Sigma_S^{(0)}$, the total positive charge density $\rho(d)$ in the diffuse layer screens the negative surface charge Σ. By integrating $\rho(d)$ across the diffuse layer, we obtain the equivalent surface charge density $\Sigma_D^{(0)}$ of the diffuse layer. In equilibrium, the EDL consisting of charged surface sites, Stern layer, and diffuse layer is electroneutral, that is, $\Sigma_S^{(0)} + \Sigma_d^{(0)} = -\Sigma$.

The electric potential at the inner limit of the diffuse layer is usually identified with the ζ-potential at the plane of shear (e.g., Leroy et al., 2008; Bücker & Hördt, 2013a). Due to the space charge ρ, the electric potential $U_a^{(0)}$ in the electrolyte decays from ζ at the solid-liquid interface to zero in the bulk electrolyte. Note that in the simplified model sketched in Figure 1, the (equilibrium) potential in the Stern layer $U_S^{(0)}$ is equal to ζ.

2.2. Basic Equations

2.2.1. Bulk Electrolyte and Diffuse Layer

The bulk electrolyte is characterized by the ion valences $z_\pm$, mobilities $\mu_\pm$, and bulk concentrations $C_\pm^\infty$, as well as the relative permittivity ϵ_a. For the sake of simplicity, we assume that the mobilities of cations (subindex +) and anions (subindex −) are equal, that is, $\mu_+ = \mu_- = \mu$, and limit our treatment to monovalent electrolytes, that is, $z_\pm = \pm 1$. In the case of a dilute solution, the electrical conductivity of the bulk electrolyte is then given by $\sigma_a = 2e\mu C_\pm^\infty$.

Spatial and temporal variations of the ion concentrations $C_\pm(\mathbf{r}, t)$ and the electrical potential $U_a(\mathbf{r}, t)$ in the solution, that is, in the diffuse layer and the bulk electrolyte, are controlled by the steady state Nernst-Planck, mass continuity, and Poisson equations (e.g., Garcia et al., 1985):

$$\mathbf{J}_\pm(\mathbf{r}, t) = -D\nabla C_\pm(\mathbf{r}, t) - z_\pm \mu C_\pm(\mathbf{r}, t)\nabla U_a(\mathbf{r}, t), \tag{1}$$

$$\nabla \mathbf{J}_\pm(\mathbf{r}, t) = -\partial_t C_\pm(\mathbf{r}, t), \tag{2}$$

$$\nabla^2 U_a(\mathbf{r}, t) = -\frac{e}{\epsilon_0 \epsilon_a}\left[C_+(\mathbf{r}, t) - C_-(\mathbf{r}, t)\right]. \tag{3}$$

Here, D denotes the diffusion coefficient, $e = 1.602 \times 10^{-19}$ C is the elementary charge, and $\epsilon_0 = 8.85 \times 10^{-12}$ F/m is the vacuum permittivity. In absence of specific interaction between the different ion species, the Einstein relation $D = \mu k_B T/e$ can be used to connect diffusion coefficient and mobility of the ions. Here, $k_B = 1.381 \times 10^{-23}$ J/K is Boltzmann's constant, and T is the absolute temperature. The current densities $\mathbf{J}_\pm$ defined by the steady state Nernst-Planck equation (1) consider diffusion $-D\nabla C_\pm$ and electromigration $-z_\pm \mu C_\pm \nabla U_a$ ion fluxes.

If the system is excited by a time-harmonic electric field $E_0 e^{i\omega t}$, where ω and t denote angular frequency and time, respectively, the ion concentrations $C_\pm(\mathbf{r}, t)$ can be expressed by the sums of the static equilibrium concentrations $C_\pm^{(0)}$ and perturbation concentrations $\delta C_\pm$ (e.g., Garcia et al., 1985):

$$C_\pm(\mathbf{r}, t) = C_\pm^{(0)}(\mathbf{r}) + \delta C_\pm(\mathbf{r}, \omega) \cdot e^{i\omega t}. \tag{4}$$

The electrical potential $U_a(\mathbf{r}, t)$ can also be decomposed into the static equilibrium potential $U_a^{(0)}$ and the perturbation $|\delta U_a| \ll U_a^{(0)}$:

$$U_a(\mathbf{r}, t) = U_a^{(0)}(\mathbf{r}) + \delta U_a(\mathbf{r}, \omega) \cdot e^{i\omega t}. \tag{5}$$

By inserting equations (4) and (5) into equations (1) through (3) and Fourier-transforming the resulting system, the problem can be decomposed into a static part and a frequency-dependent part (e.g., Chew & Sen, 1982b, 1982a). While the frequency-dependent part couples to the static solution, the static part can be solved independently.

To obtain the static part of the system, we set $\delta C_\pm, \delta U_a, \partial_t = 0$. After a few additional manipulations, this yields the Boltzmann-distributed equilibrium ion concentrations (Chew & Sen, 1982b)

$$C_\pm^{(0)}(\mathbf{r}) = C_\pm^\infty \exp\left[-\frac{z_\pm e}{k_B T} U_a^{(0)}(\mathbf{r})\right] \tag{6}$$

and the Poisson-Boltzmann equation (e.g., Chew & Sen, 1982b)

$$\nabla^2 U_a^{(0)}(\mathbf{r}) = -\kappa^2 \frac{k_B T}{e} \sinh\left[\frac{e}{k_B T} U_a^{(0)}(\mathbf{r})\right], \tag{7}$$

where $\kappa = \left[2e^2 C_{\pm}^{\infty}/(\varepsilon_0 \varepsilon_f k_B T)\right]^{1/2}$ is the inverse Debye screening length. Together with the boundary conditions discussed below, equations (6) and (7) describe the equilibrium ion concentrations $C_{\pm}^{\infty}$ and the static electrical potential $U_a^{(0)}$ in the diffuse layer and the bulk electrolyte.

In order to obtain the solution of the frequency-dependent system under the influence of a weak external field $E_0 \exp(i\omega t)$, the steady state Nernst-Planck equation (1) is inserted into the continuity equation (2), Fourier-transformed and linearized, which gives (e.g., Chew & Sen, 1982a)

$$\begin{aligned} i\omega \delta C_{\pm}(\mathbf{r},\omega) =& \nabla \left\{ D \nabla \delta C_{\pm}(\mathbf{r},\omega) \right. \\ & \left. + \mu z_{\pm} \left[C_{\pm}^{(0)}(\mathbf{r}) \nabla \delta U_a(\mathbf{r},\omega) + \delta C_{\pm}(\mathbf{r},\omega) \nabla U_a^{(0)}(\mathbf{r}) \right] \right\} + \mathcal{O}(E_0^2). \end{aligned} \tag{8}$$

The frequency-dependent perturbation concentrations of the two ion species and the potentials are coupled to each other by the Fourier-transformed Poisson equation (e.g., Chew & Sen, 1982a)

$$\nabla^2 \delta U_a(\mathbf{r},\omega) = -\frac{e}{\varepsilon_0 \varepsilon_r} \left[\delta C_+(\mathbf{r},\omega) - \delta C_-(\mathbf{r},\omega) \right]. \tag{9}$$

Equations (8) and (9) constitute three coupled PDEs that describe the spatial variations of the perturbation quantities. As the boundary conditions at the solid surface link the solution in the electrolyte to the corresponding solutions in the Stern layer and the interior of the solid, we will discuss the boundary conditions further below.

2.2.2. Stern Layer

The Stern layer is modeled as a thin layer situated at the solid-liquid interface. In absence of an external excitation, the surface-charge density $\Sigma_S^{(0)}$ in this layer is uniform. Under the influence of the electrical field $E_0 \exp(i\omega t)$, the counterions move along the surface, but no charge exchange with the electrolyte nor the solid is considered. We describe the surface-charge density in the Stern layer in terms of the constant equilibrium value $\Sigma_S^{(0)}$ and the perturbation $|\delta\Sigma_S| \ll \Sigma_S^{(0)}$, such that

$$\Sigma_S(\mathbf{r}_S, t) = \Sigma_S^{(0)} + \delta\Sigma_S(\mathbf{r}_S,\omega) \exp(i\omega t), \tag{10}$$

where $\mathbf{r}_S$ denotes the position vector in local coordinates along the solid-liquid interface. Adopting the treatment of the bound surface-charge densities on spherical particles proposed by Schwarz (1962) and Schurr (1964), the perturbation of the surface-charge density in the Stern layer is controlled by

$$i\omega \delta\Sigma_S(\mathbf{r}_S,\omega) = \nabla_S \left[D_S \nabla_S \delta\Sigma_S(\mathbf{r}_S,\omega) + \mu_S \Sigma_S^{(0)} \nabla_S \delta U_S(\mathbf{r}_S,\omega) \right] + \mathcal{O}(E_0^2), \tag{11}$$

where ∇_S is the surface Laplacian operating on functions defined on the geometrical boundary (also known as Laplace-Beltrami operator), μ_S is the mobility, D_S is the diffusion coefficient, and δU_S is the perturbation potential in the Stern layer. Note that equation (11) is the surface equivalent of equation (8) describing diffusion and electromigration surface-flux densities within the Stern layer. Only the third term on the right-hand side of equation (8) has no equivalent because the constant potential results in a vanishing tangential electrical field $-\nabla_S U_S^{(0)}$.

For spherical particles of radius a centered at the origin of the spherical coordinate system (r, θ, ϕ) and an excitation parallel to the polar axis $\theta = 0$, equation (11) takes the form (e.g., Schurr, 1964; Schwarz, 1962)

$$i\omega \delta\Sigma_S(\theta,\omega) = \frac{1}{a^2 \sin\theta} \frac{\partial}{\partial\theta} \left[D_S \sin\theta \frac{\partial}{\partial\theta} \delta\Sigma_S(\theta,\omega) + \mu_S \Sigma_S^{(0)} \sin\theta \frac{\partial}{\partial\theta} \delta U_S(\theta,\omega) \right]. \tag{12}$$

There is no particular surface equivalent of Poisson's equation (9). Instead, the continuity of the electrical potential at the solid surface (in conjunction with the vanishing thickness of the Stern layer) directly couples δU_S and the surface-charge density $\delta\Sigma_S$ to the adjacent perturbation potentials in electrolyte and solid.

2.2.3. Solid Dielectric

The solid dielectric has a relative permittivity ε_i and zero electrical conductivity. The spatial variation of the potential within the solid is governed by the Laplace equation $\nabla^2 U_i(\mathbf{r}, t) = 0$. In equilibrium, the static electrical potential $U_i^{(0)}$ must be equal to the (constant) ζ-potential on the surface, and $U_i^{(0)}$ must be constant throughout the solid. The Fourier-transformed frequency-dependent Laplace equation writes

$$\nabla^2 \delta U_i(\mathbf{r},\omega) = 0, \tag{13}$$

which in conjunction with the spatially varying surface potential $\delta U_S(\mathbf{r}_S,\omega)$ determines the perturbation potential $\delta U_i(\mathbf{r},\omega)$ within the solid.

2.3. Boundary Conditions

At far distances d from the surface, the static background potential in the electrolyte should approach zero, that is,

$$U_a^{(0)} \underset{d\to\infty}{\longrightarrow} 0. \tag{14}$$

At the surface, we take advantage of our knowledge of the constant potential $U_i^{(0)}$ inside of the solid (see above) and use the continuity of the displacement current to define the Neumann boundary condition

$$-\epsilon_0\epsilon_a \nabla U_a^{(0)}\Big|_{\text{surface}} \cdot \mathbf{n} = \Sigma + \Sigma_S^{(0)}, \tag{15}$$

where $\mathbf{n}$ denotes the unit normal vector to the solid surface (pointing out of the solid into the electrolyte) and $\Sigma + \Sigma_S^{(0)} = -\Sigma_d^{(0)}$ is the net surface-charge density. The boundary conditions on the equilibrium ion concentrations $C_\pm^{(0)}$ are implicit to equation (6).

The perturbation potential at far distances d from the surface must be equal to values corresponding to the external electrical field, that is,

$$\delta U_a(\mathbf{r},\omega) \underset{d\to\infty}{\longrightarrow} -\mathbf{E}_{\text{ext}}(\mathbf{r}) \cdot \mathbf{r}, \tag{16}$$

while the ion concentrations should approach their bulk values, that is,

$$\delta C_\pm(\mathbf{r},\omega) \underset{d\to\infty}{\longrightarrow} 0. \tag{17}$$

At the surface of the solid, the solutions for the three model domains—electrolyte, Stern layer, and solid—are pieced together. The continuity of the electrical potential demands the three perturbation potentials to be equal at any point $\mathbf{r}_S$ on the surface, that is,

$$\delta U_i(\mathbf{r}_S,\omega) = \delta U_S(\mathbf{r}_S,\omega) = \delta U_a(\mathbf{r}_S,\omega). \tag{18}$$

We assume that on the time scales of interest, ions of the solution do not engage in surface reactions; thus, they are neither produced nor consumed, and the normal fluxes through the surface are zero, that is,

$$\left\{-D\nabla\delta C_\pm(\mathbf{r},\omega) - \mu z_\pm \left[C_\pm^{(0)}(\mathbf{r},\omega)\nabla\delta U_a(\mathbf{r},\omega) + \delta C_\pm(\mathbf{r},\omega)\nabla U_a^{(0)}(\mathbf{r},\omega)\right]\right\}\Big|_{\mathbf{r}=\mathbf{r}_S} \cdot \mathbf{n} = 0. \tag{19}$$

The continuity of the displacement current implies that (e.g., Schwarz, 1962)

$$\left[-\epsilon_0\epsilon_a\nabla\delta U_a(\mathbf{r},\omega) + \epsilon_0\epsilon_i\nabla\delta U_i(\mathbf{r},\omega)\right]\Big|_{\mathbf{r}=\mathbf{r}_S} \cdot \mathbf{n} = \delta\Sigma_S(\mathbf{r}_S), \tag{20}$$

which completes the set of boundary conditions.

3. Polarization of Spherical Grains

The model setup in the previous section describes the charge polarization of the Stern layer and the concentration polarization produced by unequal contributions of anions and cations to electrical conduction through the diffuse layer. In this section, we will study the relative importance of both polarization mechanisms for the case of dilute suspensions of dielectric spheres. Because even for spherical particles no analytical solution of the fully coupled problem is known, we first obtain a suitable analytical approximation of the coupled polarization process, which combines (i) the Stern-layer polarization model by Schwarz (1962), including the correction of the corresponding relaxation time proposed by Lyklema et al. (1983), and (ii) the diffuse-layer polarization model developed by Dukhin and Shilov (1974). In order to assess the quality of our analytical model and open the possibility to model the polarization response of more complex geometrical configurations, we also present a numerical finite-element solution.

3.1. Analytical Model

At distances far from a spherical particle of radius a centered at the origin of the spherical coordinate system $\mathbf{r} = (r, \theta, \phi)$, all approximate analytical solutions take the form (e.g., Dukhin & Shilov, 1974; Maxwell, 1892; Schurr, 1964; Wagner, 1914)

$$\delta U_a(\mathbf{r}, \omega) = E_0 \left[-r + \frac{f(\omega) a^3}{r^2} \right] \cos\theta, \tag{21}$$

if the external excitation is parallel to the polar axis, that is, $\theta = 0$. The first term of this expression accounts for the potential due to the external field, and the second term describes the effective long-range dipole moment of the polarized particle. The reflection coefficient $f(\omega)$ contains the complete information on the macroscopic polarization response of the particle. For a pure Maxwell-Wagner polarization, it writes

$$f(\omega) = \frac{\sigma_i^*(\omega) - \sigma_a^*(\omega)}{2\sigma_a^*(\omega) + \sigma_a^*(\omega)}, \tag{22}$$

where $\sigma_a^*(\omega) = \sigma_a + i\omega\epsilon_0\epsilon_a$ and $\sigma_i^*(\omega) = i\omega\epsilon_0\epsilon_i$ are the complex conductivitiy of the bulk electrolyte and the nonconducting particle, respectively.

With $f(\omega)$ for one spherical particle at hand, the effective complex conductivity $\sigma^*(\omega)$ of a dilute suspension of a number of equal particles can be obtained using a generalized form of the theory by Wagner (1914)

$$\frac{\sigma^*(\omega)}{\sigma_a^*} = \frac{1 + 2\nu f(\omega)}{1 - \nu f(\omega)}, \tag{23}$$

where ν denotes the volume fraction of suspended particles. Together with the complex conductivities σ_a^* and σ_i^*, equations (22) and (23) describe the Maxwell-Wagner polarization of suspensions of dielectric particles in a medium with homogeneous complex conductivity $\sigma_a^*(\omega)$.

O'Konski (1960) included the effect of an uniform surface charge density Σ_x into this model. He found that the effect of charge carriers that move freely along the particle surface can be taken into account by adding the effective conductivity increment $\sigma_x = 2\mu_x\Sigma_x/a$ to the complex conductivity σ_i^* of the particle. According to this idea, the effective conductivity of the diffuse layer can be expressed as

$$\sigma_d = |\sigma_{d+} + \sigma_{d-}| = \frac{2\mu|\Sigma_{d+}^{(0)} - \Sigma_{d-}^{(0)}|}{a}, \tag{24}$$

where the contributions of the two types of ions to the effective conductivity of the diffuse layer are defined as

$$\sigma_{d\pm} = \frac{\pm 2\mu\Sigma_{d\pm}^{(0)}}{a}. \tag{25}$$

For sufficiently thin diffuse layers, that is, $\kappa a \ll 1$, the equivalent surface charge densities in the diffuse layer can be related to the surface charge using a variation of Bikerman's equation for the surface conductivity near a (highly) charged plane surface (e.g., Shilov et al., 2001)

$$\Sigma_{d\pm}^{(0)} = \pm\frac{2eC_\pm^\infty}{\kappa}\left[\exp\left(\mp\frac{e\zeta}{2k_BT}\right) - 1\right]. \tag{26}$$

Note that while the total charge stored in the diffuse layer is represented by the sum of both contributions, that is, $\Sigma_d^{(0)} = \Sigma_{d+}^{(0)} + \Sigma_{d-}^{(0)}$, the total surface conductivity of the diffuse layer σ_d is proportional to their difference. For a given surface charge density $\Sigma_D^{(0)}$, the ζ-potential can be obtained from

$$\zeta(\Sigma_d^{(0)}) = -\frac{2k_BT}{e}\sinh^{-1}\left(\Sigma_d^{(0)}\frac{\kappa}{4eC_\pm^\infty}\right). \tag{27}$$

This relation can readily be obtained from equation (26). Resolved for $\Sigma_d^{(0)}(\zeta)$, it is also known as Grahame equation (Grahame, 1947).

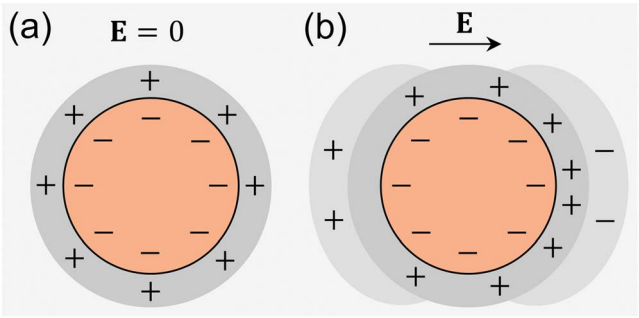

Figure 2. Sketch of the polarization of the Stern layer: (a) negatively charged particle and Stern layer in equilibrium; (b) under the influence of the external field **E**, cations in the Stern layer move along the surface, deplete on the left side and accumulate on the right side of the particle. The resulting net surface charge $\delta\Sigma_S$ causes field-induced diffuse layers of opposite charge to build up in the electrolyte next to the charged surfaces (e.g., Lyklema et al., 1983).

The surface-charge density of the Stern layer can be expressed in terms of the effective conductivity

$$\sigma_S = \frac{2\mu_S|\Sigma_S^{(0)}|}{a}. \tag{28}$$

In the present study, the partition of counterions into diffuse layer and Stern layer will be expressed in terms of the ratio $p = -\Sigma_S^{(0)}/\Sigma$. Note that this definition is slightly different from the partition coefficient $f_Q = \Sigma_S^{(0)}/(\Sigma_{d+}^{(0)} + \Sigma_S^{(0)})$ introduced by Leroy and Revil (2004).

3.1.1. Stern-Layer Polarization

If the entire counter charge is located in the Stern layer (i.e., $p = 1$), and no diffuse layer is present (i.e., $\Sigma_d^{(0)}, \zeta = 0$), the low-frequency response of the particle is caused by the polarization of the Stern layer only (see Figure 2). In the thin double layer limit, that is, $\kappa a \ll 1$, the solution of the polarization problem can be approximated as done by Schwarz (1962). In terms of the reflection coefficient f defined in equation (21), the final result obtained by Schwarz (1962) can be expressed as (from his equation 13)

$$f_S(\omega) = \frac{\sigma_S^*(\omega) - \sigma_a^*(\omega)}{2\sigma_a^*(\omega) + \sigma_S^*(\omega)}, \tag{29}$$

where σ_S^* is the effective complex conductivity of the spherical particle, which writes (from Schwarz, 1962, equations 14 and 16)

$$\sigma_S^*(\omega) = \sigma_S \frac{i\omega\tau_S}{1 + i\omega\tau_S} + i\omega\varepsilon_0\varepsilon_i. \tag{30}$$

Note that the particle is assumed to be nonconducting, that is, $\sigma_i = 0$. The relaxation time of the Stern-layer polarization τ_S can be expressed as (Lyklema et al., 1983, equation 36)

$$\tau_S = \frac{a^2}{2D_S M}, \tag{31}$$

where the coefficient M defined as (Lyklema et al., 1983, equation 34)

$$M = 1 + \frac{\kappa\Sigma_S^{(0)}}{2eC_\pm^\infty \cosh[e\zeta/(2k_BT)]} \tag{32}$$

accounts for the coupling of the charges in the Stern layer to the electrolyte, which had not been considered in the original model by Schwarz (1962).

Because $\zeta = 0$ if $p = 1$, there is no equilibrium diffuse layer, and the polarization response is only due to the polarization of the Stern layer, first term in equation (30), and the Maxwell-Wagner polarization caused by the conductivity and permittivity contrasts between particle and electrolyte.

3.1.2. Diffuse-Layer Polarization

In the opposite case, in which no Stern layer exists (i.e., $p = 0$) and the entire counter charge is located in the diffuse layer, only the diffuse layer polarizes (see Figure 3). This scenario has been treated by Dukhin and Shilov (1974) for the limit of thin diffuse layers. If electro-osmotic effects are neglected; that is, in the limit of an infinitely large fluid viscosity, the result of the classical Dukhin-Shilov theory can be expressed in terms of the reflection coefficient (e.g., Grosse & Shilov, 1996; Shilov et al., 2001)

$$f_d(\omega) = \frac{2Du(\zeta) - 1}{2Du(\zeta) + 2} - \frac{3S}{2}\frac{(\sigma_{d+} - \sigma_{d-})^2}{\sigma_a^2[2Du(\zeta) + 2]^2}\left[1 - \frac{i\omega\tau_\alpha}{1 + \sqrt{i\omega 2\tau_\alpha/S} + i\omega\tau_\alpha}\right], \tag{33}$$

where $Du(\zeta) = \sigma_d/(2\sigma_a)$ is the Dukhin number. The coefficient S, which appears in the expression for f_d, writes

$$S = \frac{[Du(\zeta) + 1]\,\sigma_a^2}{(\sigma_{d+} + \sigma_a)(\sigma_{d-} + \sigma_a)} \tag{34}$$

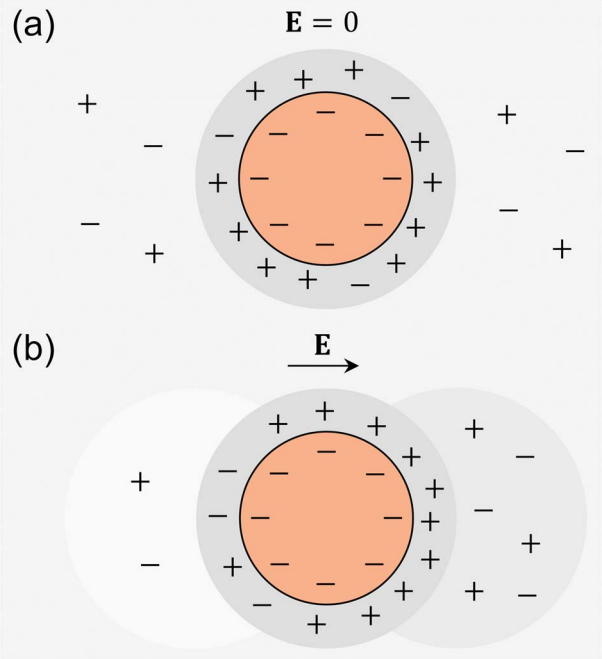

Figure 3. Sketch of the polarization of the diffuse layer: (a) negatively charged particle, diffuse layer, and bulk electrolyte in equilibrium; (b) under the influence of the external field **E**, the high effective conductivity of the diffuse layer leads to an accumulation of positive charge on the right side and negative charge on the left side of the particle. In addition, unequal migration flux densities of cations and anions through the diffuse layer are counterbalanced by an electroneutral salinity gradient that builds up next to the particle.

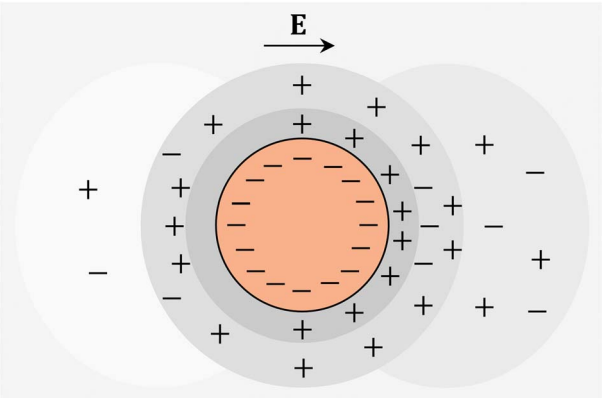

Figure 4. Sketch of the coupled polarization of Stern and diffuse layer: Due to the presence of a diffuse layer, the net surface density in the polarized Stern layer $\delta\Sigma_S$ is larger than in the case without diffuse layer (Lyklema et al., 1983). In the inner part of the diffuse layer, $\delta\Sigma_S$ attracts opposite charges (here positive on the right and negative on the left side of the particle). In the outer part, the charge in the diffuse layer changes its sign, which compensates for the high effective conductivity of this layer (as in Figure 3). The salinity gradient in the electrolyte next to the particle is a result of the unequal migration flux densities of cations and anions through the diffuse layer.

and the time constant is defined as $\tau_\alpha = a^2 S/(2D)$. The effective conductivity of the suspension can be obtained by substituting f by f_d in equation (23). Note that this formulation only accounts for the polarization of the diffuse layer; an extension including Maxwell-Wagner polarization can be found in Shilov et al. (2001).

3.1.3. Coupled Polarization

For any value $0 < p < 1$, the counter charges are distributed over Stern and diffuse layer, which leads to a simultaneous polarization of both parts of the EDL (see Figure 4). As argued by Lesmes and Morgan (2001), the coupled polarization can be approximated by a superposition of the individual responses, that is, by adding the effective complex dielectric constants of the particle (or the corresponding effective complex-conductivity increments). In order to obtain an effective conductivity increment describing the diffuse-layer polarization, we rearrange equation (22) as follows:

$$\sigma_d^*(\omega) = \sigma_a^*(\omega)\frac{1 + 2f_d(\omega)}{1 - f_d(\omega)}. \tag{35}$$

The effective conductivity σ_S^*, which accounts for Stern-layer and Maxwell-Wagner polarization, is given by equations (30) through (32), and, thus, the total effective conductivity of the particle including all three mechanisms writes

$$\sigma_c^*(\omega) = \sigma_d^*(\omega) + \sigma_S^*(\omega) = \sigma_d^*(\omega) + \sigma_S\frac{i\omega\tau_S}{1 + i\omega\tau_S} + i\omega\epsilon_0\epsilon_i. \tag{36}$$

Note that this expression is almost the same as the one obtained by Schurr (1964) except for the decrease of τ_S by the factor M and the substitution of σ_d by $\sigma_d^*(\omega)$, that is, including the frequency-dependent contribution of the diffuse layer defined by equations (33) through (35).

The new coupled model described here is also similar to the one proposed by Lesmes and Morgan (2001), from which it differs with regard to (i) the relaxation time of the Stern layer τ_S, where we use the correction by Lyklema et al. (1983); (ii) the low-frequency contribution σ_S of the Stern layer (their equations 5 and 6), which we do not consider because it contradicts the assumption of a strongly bound Stern-layer; and (iii) the selection of the model describing the diffuse-layer polarization, where we use the Dukhin-Shilov theory instead of the model by Fixman (1980). Fixman's assumption that the coion contribution to the surface conductivity can be ignored for sufficiently high ζ-potentials does not hold for the range of ζ-potentials studied here. We found that this simplification significantly affects the real part of the complex conductivity (not shown here for brevity).

3.2. Numerical Model

Figure 5 shows the geometrical setup used for the numerical modeling. The dielectric particle of radius a is centered at the origin of coordinates, and the external electric field is imposed in x direction, that is, $\mathbf{E}_{\text{ext}} = E_0\mathbf{e}_x$, where $\mathbf{e}_x$ denotes the unit vector in x direction. Due to the cylindrical symmetry of the problem, the numerical simulation can be carried out on the two-dimensional model domain in Carthesian coordinates $\mathbf{r} = (x, y)$ marked in red in Figure 5.

We use the finite-element software COMSOL Multiphysics to successively obtain the static and the frequency-dependent solution. We first

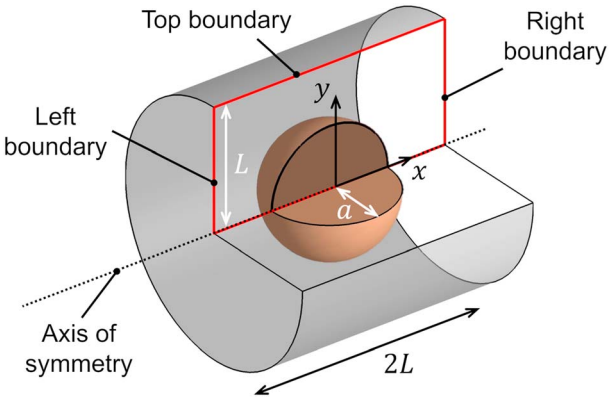

Figure 5. Three-dimensional sketch of the geometrical setup used for the numerical simulation of the polarization around spherical particles. The particle of radius a is enclosed by a cylinder of radius L and height $2L$, which represents the electrolyte. The red rectangle marks the actual two-dimensional model domain.

solve the Poisson-Boltzmann equation (7), which contains $U^{(0)}(\mathbf{r})$ as only unknown variable. For the numerical implementation, boundary conditions (14) and (15) are translated as follows: $U^{(0)} = 0$ on the left, right, and top boundary; $[\varepsilon_0\varepsilon_i\nabla U_i^{(0)} - \varepsilon_0\varepsilon_a\nabla U_a^{(0)}]\mathbf{n} = -\Sigma_d^{(0)}$ on the particle surface; and $\partial U(0)/\partial_y = 0$ on the axis of symmetry. The static background ion concentrations are computed by inserting $U_a^{(0)}$ into equation (6).

Subsequently, we solve the frequency-dependent part described by equations (8), (9), (11), and (13) and the boundary conditions (16) through (20). For the numerical solution, the latter are adjusted as follows: $\delta n_\pm = 0$ and $\delta U_a = \pm E_0 L$ on the left and right boundary, respectively; $\mathbf{J}_\pm = 0$ and $\partial\delta U/\partial_y = 0$ on top boundary and on the axis of symmetry; unchanged on the particle surface. While the static solution only needs to be computed once for each set of model parameters (i.e., a, Σ, and p), the frequency-dependent problem has to be solved for each value of the angular frequency ω separately.

Because bulk values are implicitly assumed on the left, right, and top boundary, these boundaries must be placed sufficiently far away from the particle surface, where the polarization is expected to cause nonzero perturbations. As a trade-off between precision and computational cost, we define a standard domain size of $L = 10a$. For more technical details on the implementation, see the appendix.

The effective conductivity of the model can be obtained from the numerical integration of the total ion flux densities through the left (or likewise the right) boundary, that is,

$$\sigma^*_{\mathrm{mod}} = \frac{2}{E_0 L^2}\int_0^L \left[\mathbf{J}_+(y) + \mathbf{J}_-(y)\right]\mathbf{e}_x y dy, \tag{37}$$

where the term ydy accounts for the area element of the boundary and the factor $2/L^2$ stems from the normalization with the total area.

The standard domain size is $L = 10a$ and corresponds to a rather small volume fraction of dielectric particles. Therefore, we scale the modeled effective conductivities $\sigma^*_{\mathrm{mod}}(\omega)$ to a more realistic volumetric content of $\nu = 0.4$ using the mixing rule defined in equation (23) with

$$f(\omega) = \frac{1}{\nu_{\mathrm{mod}}}\frac{\sigma^*_{\mathrm{mod}}(\omega) - \sigma^*_a(\omega)}{\sigma^*_{\mathrm{mod}}(\omega) + 2\sigma^*_a(\omega)}. \tag{38}$$

3.3. Comparison of Analytical and Numerical Solution

Unless otherwise stated, the following parameter values are used to obtain both numerical and analytical results: The relative permittivities are $\varepsilon_a = 80$ for the aqueous electrolyte and $\varepsilon_i = 4.5$ for the solid, which is a typical value for quartz sand (e.g., Robinson & Friedman, 2003). The uniform ion mobility is $\mu = 5 \cdot 10^{-8}$ $\mathrm{m}^2/(\mathrm{Vs})$, which is approximately equal to the mobility of the sodium cation (e.g., Atkins & De Paula, 2013) and will be used for both ion species in the electrolyte. The mobility of the counterions in the Stern layer is only 10% of the ion mobility in the bulk electrolyte, that is, $\mu_S = \mu/10$. This value corresponds to the reduction of the cation mobility in the Stern layer inferred for K^+ on latex surfaces by Zukoski and Saville (1986) and for Na^+ on clay surfaces by Revil and Glover (1998) and Revil et al. (1998). For near-neutral pH of the solution and ion concentrations in the bulk electrolyte of $C_\pm^\infty = 1\ \mathrm{mol/m}^2$, it is adequate to assume a surface charge density of $\Sigma = -0.01\ \mathrm{C/m}^3$ (e.g., Kosmulski, 2006). The absolute temperature of $T = 293$ K (room temperature) and the above-mentioned volumetric content of $\nu = 0.4$ complete the set of standard model parameters.

Figure 6 displays the conductivity spectra of a suspension of spherical particles of radius $a = 5\,\mu\mathrm{m}$ for six values of p between 0 and 1. The effective conductivity of the mixture σ^* is expressed in terms of the corresponding real (σ') and imaginary (σ'') parts. In Figure 6a, we observe a continuous decrease of σ' with increasing p. This means that the surface conductivity due to counterions in the diffuse layer is much larger than the one of the Stern layer. This is due, on the one hand, to the significantly reduced mobility of the counterions in the Stern layer, which affects all frequencies equally. On the other hand, at low frequencies,

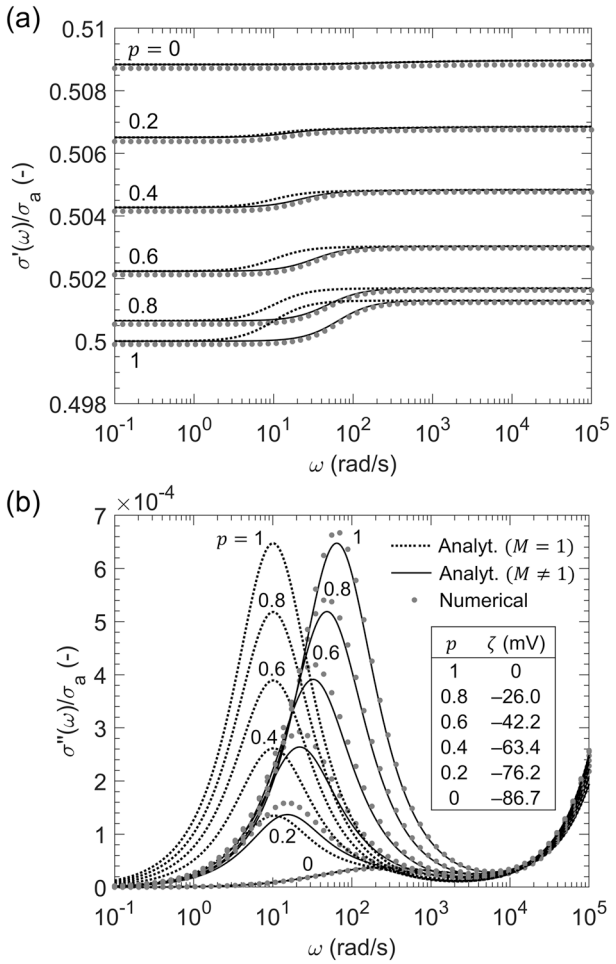

Figure 6. Complex-conductivity spectra of a suspension of dielectric particles of radius $a = 5\,\mu m$ at different ratios $p = -\Sigma_S^{(0)}/\Sigma$, that is, the surface charge in the Stern layer increases with p. Complex-valued conductivities in terms of real (a) and imaginary (b) parts normalized to the bulk conductivity σ_a. Numerical results (gray circles) are displayed along with the corresponding analytical models according to equation (36) using the simple relaxation time after Schwarz, (1962; $M = 1$ in equation (31), dotted line) and using the corrected relaxation time after Lyklema et al. (1983; $M \neq 1$, solid line). The values of ζ shown in (b) are computed from equation (27).

the Stern layer is completely polarized and does not contribute to the DC conductivity because we assume that it cannot exchange ions with the bulk electrolyte. However, the Stern layer does contribute to the high-frequency limit of σ', that is, at frequencies larger than the characteristic frequency of the Stern-layer polarization. The higher p and thus the surface conductivity σ_S, the larger becomes the difference between high- and low-frequency limits of σ', which is largest in the case of a pure Stern-layer polarization ($p = 1$). In contrast, in the case of a sole diffuse-layer polarization ($p = 0$), we hardly recognize any variation of σ' with the angular frequency.

The peak imaginary conductivity σ'' (Figure 6b) increases almost linearly with p, that is, the charge density in the Stern layer. For the same surface-charge densities, the Stern-layer polarization ($p = 1$) results in a maximum of σ'', which is approximately an order of magnitude larger than the peak produced by the corresponding diffuse-layer polarization ($p = 0$). From Figure 7, which shows a close-up of the small imaginary conductivities generated in the case of a depopulated Stern layer, it is evident that even a small fraction of 20% of positive charge located in the Stern layer produces a stronger response than the other 80% located in the diffuse layer. It is worth mentioning that the polarization magnitude (here in terms of the maximum of σ'') largely varies with the mobility of the counterions in the Stern layer. In a separate analysis, we observed a difference between the magnitudes of the two polarization processes of 2 orders of magnitude when a larger mobility of $\mu_S = \mu/2$ was assumed (not shown). This observation is in agreement with the

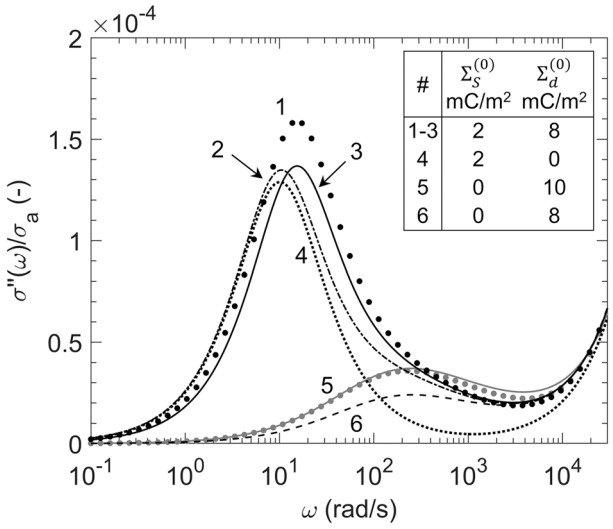

Figure 7. Numerical (filled circles) and analytical (lines) imaginary conductivity spectra for small surface charge densities $\Sigma_S^{(0)}$ in the Stern layer. Analytical curves are calculated from equation (36), using the values of $\Sigma_S^{(0)}$ and $\Sigma_D^{(0)}$ given in this Figure. Curve 1, numerical solution for the coupled Stern and diffuse-layer polarization; curves 2 and 3, analytical solution for the coupled Stern and diffuse-layer polarization using $M = 1$ and $M \neq 1$ in equation (31), respectively; curve 4, analytical solution for a pure Stern-layer polarization using $M = 1$; curves 5 and 6, numerical and analytical solutions for a pure diffuse-layer polarization and two different surface charge densities $\Sigma_D^{(0)}$ in the diffuse layer.

results obtained earlier by Lesmes and Morgan (2001) and confirms their conclusion that the Stern-layer polarization produces a much stronger frequency dispersion than the diffuse-layer polarization.

For sufficiently small values of p, Figure 7 also shows that the contribution of the diffuse-layer polarization results in a slight increase of the polarization magnitude and the characteristic angular frequency (curves 1 and 3) as compared to the pure Stern-layer polarization (curve 4). The latter is related to the higher characteristic frequency of the diffuse-layer relaxation as a consequence of the shorter relaxation time, here $\tau_\alpha \approx \tau_S/2$ because $S \approx 1$.

The comparison of the corresponding curves in Figures 6 and 7 also serves as a mutual validation of our finite-difference implementation and the new analytical approximation for the coupled polarization response. For angular frequencies between 0.1 and 10^4 mrad/s, the relative deviation between analytical and numerical results is <0.3% in the real part and <20% in the imaginary part of the effective conductivity. Here, the analytical approximation clearly underestimates the polarization magnitude. A good agreement, however, is observed between the characteristic frequency, that is, the angular frequency at which the σ'' peaks are observed. Apart from the underestimated polarization magnitude, the good agreement between numerical and analytical curves confirms the approach to model the coupled polarization process by a simple superposition of the individual responses of Stern and diffuse layer.

4. Membrane Polarization

Besides the polarization of Stern and diffuse layer around grains, the polarization of ion-selective pore constrictions can also cause a low-frequency dispersion of the complex conductivity. In the present section, we study this membrane-polarization mechanism based on an alternating series of wide and narrow cylinders. The cylinder walls are negatively charged and covered by an EDL consisting of a Stern and a diffuse layer, both contributing to the macroscopic polarization of the system. In order to assess their relative contributions, effective conductivity spectra are computed for varying charge densities in the two layers. Because no analytical model is available for the coupled response in this geometry, we resort to the numerical finite-element implementation validated in the previous section. We also show that after a slight modification presented here, the analytical membrane-polarization model proposed by Bücker and Hördt (2013a) reproduces the numerical results for the sole diffuse-layer polarization fairly well.

4.1. Analytical Model for Diffuse-Layer Polarization

Bücker and Hördt (2013a) considered the sequence of wide and narrow pores sketched in Figure 8. The pores are characterized by their radii R_i and lengths L_i; the indices 1 and 2 denote properties of the wide and the narrow pore, respectively. A nonzero ζ-potential at the cylinder walls causes diffuse layers to build up. According to Bücker and Hördt (2013a), upon excitation by an external electrical field, the electrical current parallel to the symmetry axis will be controlled by the mean ion concentrations

$$b_{\pm,i} = \frac{2\pi}{C_\pm^\infty A_1} \int_0^{R_i} r C_{\pm,i}^{(0)}(r) dr. \tag{39}$$

These mean ion concentrations are averaged over the pore cross-section and normalized with the bulk ion concentration $C_\pm^\infty$. An additional normalization with the area of the wide pore $A_1 = \pi R_1^2$ accounts for the reduction of the total current through the narrow pore due to the reduced cross-section (see Bücker & Hördt, 2013a).

For sufficiently small ζ-potentials, that is, $\zeta \ll k_B T/e$, the radial variation of the electrical potential in the pore can be approximated by solving the linearized Poisson-Boltzmann equation in cylindrical coordinates,

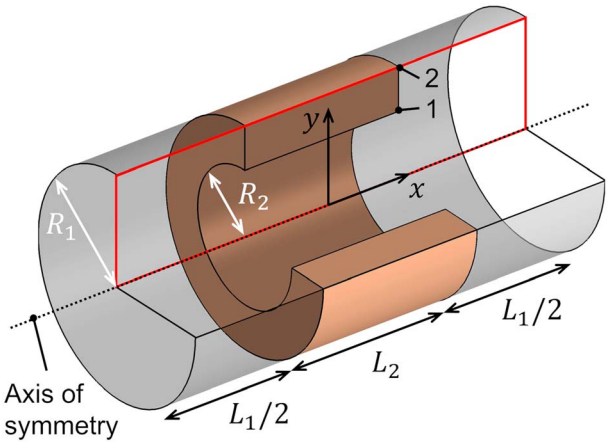

Figure 8. Three-dimensional sketch of the geometrical setup used for the numerical simulation of membrane polarization in a pore constriction. The two wide cylinders of length $L_1/2$ and radius R_1 and the narrow cylinder of length L_2 and radius R_2 are saturated with electrolyte solution. The volume around the narrow cylinder belongs to the nonconducting matrix with dielectric constant ϵ_i. The red rectangle marks the actual two-dimensional model domain.

which gives (Hunter, 1981; Bücker & Hördt, 2013a)

$$U_a^{(0)}(r) = \zeta \frac{J_0(i\kappa r)}{J_0(i\kappa R)}, \tag{40}$$

where J_0 is the Bessel function of the first kind and order zero. The radial variation of the ion concentrations $C_{\pm,i}^{(0)}(r)$ are obtained by inserting $U_a^{(0)}(r)$ into equation (6).

For the typically much higher ζ-potential values of up to −100 mV on silica surfaces (here, $\Sigma = -0.01$ C/m^2), the solution of the linearized Poisson-Boltzmann equation becomes imprecise. If we instead limit our treatment to sufficiently wide pore radii, that is, $\kappa R_i \ggg 1$, we can make use of Bikerman's equation 26, which is more adequate for highly charged surfaces. The dimensionless mean ion concentrations can then be approximated by

$$b_{\pm,i} \approx \frac{A_i}{A_1}\left(\frac{\pm 2\Sigma_{d\pm}^{(0)}}{eC_{\pm}^{\infty}R_i} + 1\right). \tag{41}$$

Either of these definitions of $b_{\pm,i}$, that is, equation 39 proposed by Bücker and Hördt (2013a) or equation (41) proposed here, can be used to express the effective transference numbers

$$t_{\pm,1} = \frac{b_{\pm,i}}{b_{+,i} + b_{-,i}}. \tag{42}$$

By means of this approximation, the three-dimensional cylindrical pore system is collapsed to a sequence of one-dimensional pores, the frequency-dependent impedance of which was derived by Marshall and Madden (1959). Following Bücker and Hördt (2013b) and Bücker et al. (2017), the Marshall-Madden impedance can be written as

$$Z(\omega) = \frac{2}{\sigma_a}\left[\frac{L_1}{b_{+,1}+b_{-,1}} + \frac{L_2}{b_{+,2}+b_{-,2}} + \frac{8D\left(t_{+,1}-t_{+,2}\right)^2}{\frac{L_1}{\tau_1}\sqrt{i\omega\tau_1}\coth\sqrt{i\omega\tau_1} + \frac{L_2}{\tau_2}\sqrt{i\omega\tau_2}\coth\sqrt{i\omega\tau_2}}\right], \tag{43}$$

where the frequency dependence is controlled by the two time constants

$$\tau_i = \frac{L_i^2}{2D}S_i \quad \text{with} \quad S_i = \frac{1}{4b_{+,i}t_{-,i}}. \tag{44}$$

In order to stress the structural similarities between these two relaxation times and the relaxation time of the diffuse layer around spherical grains, we can rewrite the dimensionless mean ion concentrations $b_{\pm,i}$ defined in equation (41) in terms of a Dukhin number for cylindrical geometries, which we define as

$$Du(\zeta, R_i) = \frac{\sigma_d(R_i)}{2\sigma_a} = \frac{|\sigma_{d+}(R_i) + \sigma_{d-}(R_i)|}{2\sigma_a}. \tag{45}$$

In analogy to equation (25), the surface conductivities write $\sigma_{d\pm}(R_i) = \pm 2\mu\Sigma_{d\pm}^{(0)}/R_i$. The coefficients S_i take the form

$$S_i = \frac{A_1}{2A_i}\frac{[2Du(\zeta,R_i)+1]\sigma_a^2}{[2\sigma_{d+}(R_i)+1][2\sigma_{d-}(R_i)+1]}. \tag{46}$$

Besides the factor $A_1/(2A_i)$ and the factors 2, with which the Dukhin numbers and the individual conductivities $\sigma_{d\pm}$ are multiplied, this definition of S_i is equivalent to the definition of S in equation (34), which controls the relaxation time of the diffuse layer around spherical particles.

4.2. Numerical Model for the Coupled Polarization

The numerical modeling is carried out using COMSOL Multiphysics. Again, the cylindrical symmetry of the problem permits limiting the computation to a two-dimensional model domain (red rectangle in Figure 8).

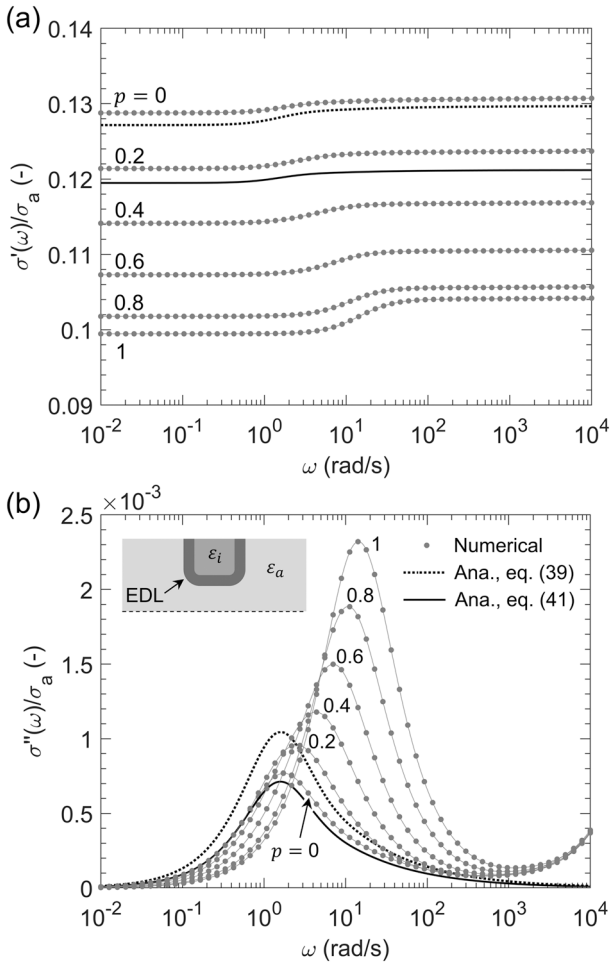

Figure 9. Complex-conductivity spectra of the membrane-polarization model for different ratios $p = -\Sigma_S^{(0)}/\Sigma$. Complex-valued conductivity in terms of real (a) and imaginary parts (b) normalized to the bulk conductivity σ_a. Numerical results (gray circles, lines are to guide the eye only) for all values of p are displayed along with the analytical models for $p = 0$ after Bücker and Hördt (2013a) using the average ion concentrations from equation (39) (dotted line) and from equation (41) (solid line). The sketch in (b) shows that the electrical double layer (EDL) is discontinuous in the wide pore. Pore lengths and radii are $L_1 = 90\,\mu\text{m}$, $L_2 = 10\,\mu\text{m}$, $R_1 = 2\,\mu\text{m}$, and $R_2 = 0.2\,\mu\text{m}$; all other parameter values are the same as in Figure 6.

The systems of PDEs describing the static and the frequency-dependent parts of the polarization problem remain unchanged, and only boundary conditions and finite-element mesh need to be adapted to the different geometry.

The boundary conditions for the static solution, that is, equations (14) and (15), merge into $U^{(0)} = 0$ on the left and right boundary; $[\varepsilon_0\varepsilon_i\nabla U_i^{(0)} - \varepsilon_0\varepsilon_a\nabla U_a^{(0)}]\mathbf{n} = -\Sigma_d^{(0)}$ on the solid-liquid interface; and $\partial U(0)/\partial_y = 0$ on the axis of symmetry and the entire top boundary. This setup represents a discontinuous EDL, which only covers the surfaces of the volume shown in brown in Figure 8. Additionally, we compute the response of a setup, where the EDL is continuous in the wide pore and the boundary condition on the corresponding parts of the top boundary writes $[-\varepsilon_0\varepsilon_a\nabla U_a^{(0)}]\mathbf{n} = -\Sigma_d^{(0)}$.

For the frequency-dependent part of the problem, the boundary conditions described in equations (16) through (20) are adjusted as follows: $\delta n_\pm = 0$ and $\delta U_a = \pm E_0 L$ on the left and right boundary, respectively; $\mathbf{J}_\pm = 0$ and $\partial\delta U/\partial_y = 0$ on the axis of symmetry and the top boundary; equations (18) through (20) remain unchanged on the solid-liquid interface. In the setup with the continuous EDL, the boundary conditions on those parts of the top boundary, which delimit the wide pore, are given by the unchanged zero-flux condition (19) and the continuity of the displacement current, which here writes $-\varepsilon_0\varepsilon_a\nabla\delta U_a(\mathbf{r}_S)\cdot\mathbf{n} = \delta\Sigma_S(\mathbf{r}_S)$.

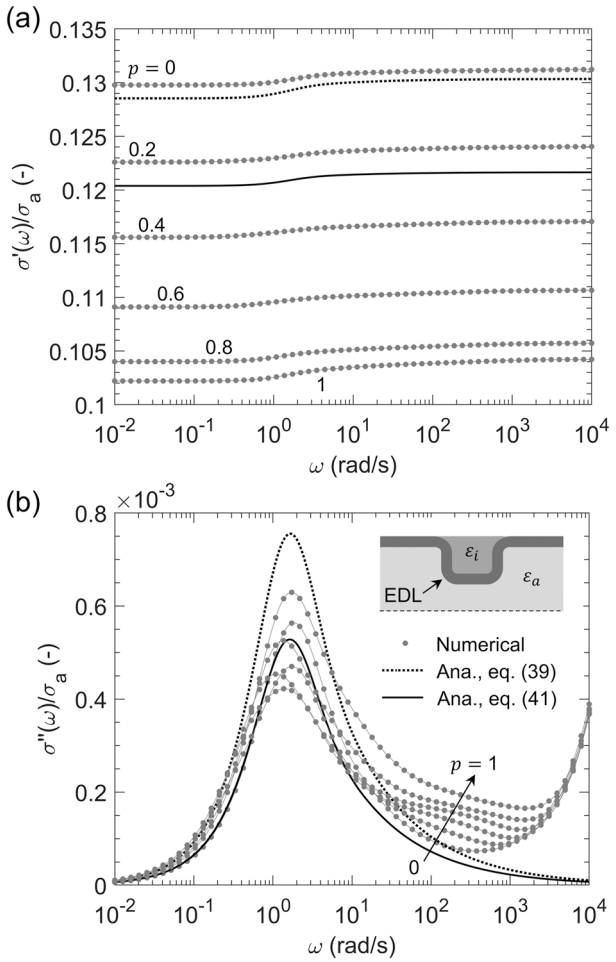

Figure 10. Complex-conductivity spectra of the membrane-polarization model with a continuous electrical double layer (EDL) in terms of the normalized real (a) and imaginary conductivity (b). Numerical results (gray circles lines are to guide the eye only) for different values of p are displayed along with the analytical models for $p = 0$ after Bücker and Hördt (2013a) using the average ion concentrations from equation (39) (dotted line) and from equation (41) (solid line). The sketch in (b) shows the continuous EDL in the wide pore; all other parameter values are the same as in Figure 9.

In order to avoid artifacts related to sharp corners covered by an EDL, the vertex 1 in Figure 8 is rounded off for the model with a discontinuous EDL, whereas the vertices 1 and 2 are rounded off for the model with a continuous EDL. In both cases, the radius of curvature is $(R_1 - R_2)/2$. For further technical details on the implementation, see the appendix.

The effective conductivity of the model can be obtained from numerically integrating the total ion flux densities through the left (or right) boundary. The resulting expression is equal to equation (37), if L substituted by R_1. In the model with the continuous EDL, the surface current through the Stern layer has to be considered, too. The corresponding conductivity increment $-2/(E_0 R_1)[D_S \partial\delta\Sigma_S/\partial x + \mu_S \Sigma_S \partial\delta U_S/\partial x]$ has to be added to σ^*_{mod}. The analytical expression for the effective conductivity writes $\sigma_{\text{eff}}(\omega) = (L_1 + L_2)/Z(\omega)$, where $Z(\omega)$ is defined in equation (43).

4.3. Comparison of Analytical and Numerical Solution

The effective-conductivity spectra obtained from the model with the discontinuous EDL are shown in Figure 9. In the analytical models (for the case $p = 0$), the absence of the EDL in the wide pore has to be taken into account by setting $b_{\pm,1} = 1$ instead of using equation (39) or (41). The length of the narrow pore $L_2 = 10\,\mu\text{m}$ was selected to match the diameter of the spherical particle treated above; the length of the wide pore $L_1 = 90\,\mu\text{m}$ as well as the two pore radii $R_1 = 2\,\mu\text{m}$ and $R_2 = 0.2\,\mu\text{m}$ were adjusted to achieve a significant polarization response. As discussed in more detail in Hördt et al. (2017), the polarization magnitude of

the model by Bücker and Hördt (2013a) largely depends on the relation between the two ratios R_1/R_2 and L_1/L_2.

In Figure 9a, we observe a similar variation of the magnitude of σ' with the ratio p as for the polarization around a spherical particle. In both cases, the surface conductivity increases σ' if the countercharges are mainly located in the diffuse layer. At low frequencies, the Stern layer polarizes and does not contribute to σ'; at high frequencies, its contribution is limited by the low ion mobility in the Stern layer (remember that $\mu_S = \mu/10$). Moreover, the variation of the imaginary part σ'' with p (Figure 9b) is similar to the one observed for the spherical particle. Again, the σ'' peak increases with the amount of countercharges located in the Stern layer, that is, with increasing p, and shifts toward higher angular frequencies.

Figure 9 also shows that computing the mean ion concentrations from equation (41) instead of equation (39) improves the agreement with the numerical solution: for $p = 0$, the relative deviations between the analytical and the numerical σ'' curves are <20% for the modified and <50% for the original model at angular frequencies <100 rad/s. Because the analytical model does not consider Maxwell-Wagner polarization, which becomes dominant at high frequencies, the misfit increases at angular frequencies >100 rad/s. The original membrane polarization model, however, matches the real part (σ') better. Here, the relative deviation between the analytical models and the numerical solution are ≈7% for the modified and <1% for the original model.

The fair overall agreement of analytical and numerical curves for $p = 0$ confirms the validity of the model developed by Bücker and Hördt (2013a) for a sole diffuse-layer polarization. The same authors also proposed a simple modification of the mean counterion concentration to take into account the contribution of the Stern layer. However, their model rather predicts a continuous decrease of the polarization magnitude with increasing p and practically a constant characteristic frequency (not shown here for brevity), indicating that the Stern-layer polarization is more complex than assumed by Bücker and Hördt (2013a).

The polarization response changes significantly if the EDL is assumed to be continuous in the wide pore (Figure 10). Here, magnitude and characteristic frequency of the main σ'' peak located around 2 rad/s decrease only slightly from $p = 0$ to $p = 0.4$ and increase not much steeper for larger values of p. In comparison to the significant variation of the main peak observed in Figure 9 for the discontinuous EDL, here, the σ'' peak remains almost unchanged. Furthermore, at frequencies between 100 and 1,000 rad/s, a smaller secondary polarization peak appears for $p > 0$ and increases monotonically with p. The real part σ' shows the usual decrease of surface conductivity with increasing p. The relative deviations between the numerical results for $p = 0$ and the two analytical models are similar to those reported above for a discontinuous EDL.

5. Discussion

The new analytical model presented here describes Maxwell-Wagner, Stern-layer, and diffuse-layer polarization around spherical grains and permits analyzing the frequency response due to a superposition of all three mechanisms. Numerical and analytical results for typical model parameters consistently confirm the results of earlier studies: The contribution of the diffuse-layer polarization to the macroscopic response is significantly smaller than the one of the Stern-layer polarization (e.g., de Lima & Sharma, 1992; Lesmes & Morgan, 2001). In most practical cases, the polarization of the diffuse layer can therefore safely be neglected.

The comparison of numerical and analytical results also confirmed the strong coupling of the surface charge in the Stern layer with charges in the electrolyte as predicted by Lyklema et al. (1983). The model proposed by Lyklema and coworkers can easily be obtained from the model by Schwarz (1962) by adjusting the relaxation time of the Stern layer: For a charge density in the Stern layer of $\Sigma_S^{(0)} \approx 0.01$ C/m^2 and a bulk ion concentration of 1 mol/m^3, equation (32) predicts a reduction of the relaxation time by a factor $M \approx 6.4$. This effect can also be interpreted in terms of an effective diffusion coefficient $D_S^{\text{eff}} = D_S M$, which in our case (i.e., $D_S = D/10$) is only a factor ≈2 smaller than the diffusion coefficient of the ions in the bulk electrolyte.

This observation is of particular interest, as it offers an explanation for the large diffusion coefficients D_S needed to adjust the model by Leroy et al. (2008) to measured complex-conductivity spectra. The model by Leroy and coworkers does not include the correction of the relaxation time proposed by Lyklema et al. (1983). Thus, it often requires the assumption of similar diffusion coefficients in Stern layer and bulk electrolyte (e.g., Leroy & Revil, 2009; Leroy et al., 2008; Revil & Florsch, 2010; Schmutz et al., 2010). Independent determinations of the diffusion coefficient in the Stern layer from experimental surface-conductivity and

particle-mobility data, however, normally result in a reduction of the counterion mobility by a factor 10 or larger (e.g., Zukoski & Saville, 1986; Revil & Glover, 1998). A recent extension of the model by Leroy et al. (2008) already considers the corrected relaxation time and successfully adjusts the polarization response of calcite precipitations on glass beads (Leroy et al., 2017). Together with our findings that support the theory by Lyklema et al. (1983), this indicates that the difference between the predictions of the two experiments could be reduced significantly, if the Stern-layer relaxation time used in the model by Leroy et al. (2008) (and subsequent studies) was replaced by the one defined in equations (31) and (32).

Although the correction of the relaxation time might be able to justify the (to date) unexplained assumption inherent to the model by Leroy et al. (2008), it also questions the often-used simple relation between relaxation time and grain size by introducing an additional dependence on chemical properties of pore fluid and solid surface: The coefficient M strongly depends on the electrolyte concentration and the surface-charge density in the Stern layer. Consequently, besides the grain diameter and the diffusion coefficient in the Stern layer, variations of experimentally determined relaxation times might partly be due to variations of these chemical parameters.

We have also applied our finite-element model to study membrane polarization, which had not been investigated in the same detail as the polarization around spherical grains before. In the limiting case of a sole diffuse-layer polarization, we found that an improved analytical formulation based on the work by Marshall and Madden (1959) and Bücker and Hördt (2013a) yields a good agreement with the numerical results. However, the analytical model does not reproduce the numerical results for the coupled polarization of diffuse and Stern layer. Consequently, the incorporation of the Stern-layer polarization in the model by Bücker and Hördt (2013a) is insufficient in its current form, and our numerical results can contribute substantially to our understanding of the role of the Stern layer in the context of membrane polarization.

Even in the pore-constriction geometry, the polarization of the Stern layer can control the frequency response, especially if the EDL is discontinuous. Certain similarities of the coupled responses of both geometries stand out—namely, the generally larger response of the Stern-layer polarization and the simultaneous increase of characteristic frequency and polarization magnitude with the surface charge in the Stern layer. However, we also observed that the particular geometrical configuration of the EDL in the pore-constriction model can largely reduce the difference between the respective magnitudes of diffuse-layer and Stern-layer polarization: If the EDL becomes continuous, the contributions of both mechanisms can become practically the same.

Although we have taken an important step toward this long-term goal, it is beyond the scope of the present study to provide an analytical model that integrates membrane polarization and the polarization around spherical grains. Nevertheless, we can put our results into a broader context and draw some preliminary conclusions regarding the relative contributions of the various polarization mechanisms.

Grain-based polarization models are best suited for the modeling of dilute suspensions of dielectric particles because they only account for grain-electrolyte interactions and largely ignore grain-grain interactions. For practical purposes, these models can even be applied to high particle concentrations, and the responses of unconsolidated granular media (e.g., Leroy et al., 2008) have been matched successfully with this type of models. For typical parameter combinations, the polarization of isolated grains is only controlled by the Stern layer, and contributions of a simultaneously occurring diffuse-layer polarization can be neglected.

With increasing degree of compaction and cementation, grain-grain interactions are expected to become more important (e.g., Lesmes & Morgan, 2001). These interactions include (i) the interaction of polarization dipoles of adjacent grains as well as (ii) percolating diffuse and Stern layers. Based on the good agreement between experimental data and the responses of grain-based polarization models, the interaction of polarization dipoles can safely be neglected. To date, the effect of percolating diffuse and Stern layers on the polarization response has only been touched in passing: For instance, Leroy et al. (2008) argue that a diffuse layer above the percolation threshold cannot polarize and only consider an increase of the low-frequency conductivity. In the same sense, they postulate that the Stern layers of adjacent particles are discontinuous because the model based on the Stern-layer polarization accurately describes experimental observations. While the result of this argumentation—the small contribution of the diffuse-layer polarization and the dominating role of the Stern layer—agrees with our findings, the physical picture should be reconsidered: Around isolated particles, the polarization of the diffuse layer is negligible, too, such that it is not necessary

to assume that the diffuse layers are percolating. In addition, we have shown that even in the case of continuous (or percolating) diffuse and Stern layers in the pore-constriction model, both layers can polarize. Consequently, the discontinuity of neither of the two layers is needed to generate a polarization response.

The similarity of the polarization response of grain-based and pore-constriction geometry indicates a gradual transition between the two models with increasing degree of compaction and cementation. As long as the EDLs are assumed to be discontinuous, the Stern layer dominates the polarization response of both models, which makes the distinction between effects related to individual grains and effects related to pore constrictions a mere question of the point of view. Our results suggest that responses caused by pore constrictions, that is, typical membrane-polarization responses, can—at least to a certain degree—be adjusted using grain-based models and vice versa. This is particularly plausible, if we consider that in granular media made of near-spherical particles, pore diameters and pore lengths are of the same order of magnitude as the typical grain sizes and thus all relaxation times are controlled by similar characteristic lengths.

6. Conclusions

We have investigated the low-frequency electrical conductivity of porous media by means of analytical and numerical models for single-grain and pore-constriction geometries. Our results allowed us to assess the relative contributions of polarization mechanisms originating from the diffuse part and the Stern layer of the EDL covering charged mineral surfaces. Because our models also include Maxwell-Wagner polarization, they are useful for a broad frequency range.

To match our numerical results, we assembled a new analytical model for the grain-based geometry by combining the Dukhin-Shilov model (Dukhin & Shilov, 1974), which accounts for the diffuse-layer polarization, with Schurr's Stern-layer polarization model (Schurr, 1964) including a correction of the Stern-layer relaxation time proposed by Lyklema et al. (1983). The corrected relaxation time, which accounts for the interaction of the charges in the Stern layer with the electrolyte solution, significantly improves the agreement of analytical and numerical results. Without the correction, untypically high diffusion coefficients of the counterions in the Stern layer have to be assumed to fit the spectral response. For typical model parameters, the relative contribution of the diffuse-layer polarization was seen to be insignificant in comparison to the large response of the Stern layer.

Our numerical results for the pore-constriction geometry agree with the analytical membrane-polarization model by Bücker and Hördt (2013a) if we relate the mean ion concentrations of the cylindrical pores to Bikerman's expression for the surface conductivity of highly charged surfaces (Bikerman, 1933) and as long as no Stern layer is considered. We also propose detailed model to describe Stern-layer polarization in a typical membrane-polarization geometry. As in the grain-based model, the diffuse layer makes a much smaller contribution to the total response than the Stern layer—at least as long as the charged surfaces are below the percolation threshold; that is, the individual EDLs are not interconnected at the system scale.

In conclusion, the responses of grain-based and pore-constriction geometries are more similar than usually assumed, particularly if the polarization of both parts of the EDL are taken into account. Below the percolation threshold, the Stern-layer dominates the macroscopic response, but as soon as the EDL becomes percolating, this dominance breaks down and both mechanisms contribute to a similar extend. More detailed studies on specific pore geometries are required to conclusively assess the relative importance of the different polarization mechanisms, but our study is a significant step toward this long-term goal and sets the basis for extensive numerical studies.

Appendix A: Numerical Implementation

The COMSOL PDE interface in coefficient form allows the definition of PDEs and systems of PDEs of the general type

$$e_a \frac{\partial^2 u}{\partial t^2} + d_a \frac{\partial u}{\partial t} + \nabla \cdot (-c\nabla u - \alpha u + \gamma) + \beta \cdot \nabla u + au = f \tag{A1}$$

with the general boundary conditions

$$-\mathbf{n} \cdot (-c\nabla u - \alpha u + \gamma) = g - qu \quad \text{and} \tag{A2}$$

$$u = s, \tag{A3}$$

where u denotes the dependent variable and $\mathbf{n}$ the inward-pointing unit normal vector.

Due to their cylindrical symmetry, the problems can be solved on two-dimensional domains (see Figures 5 and 8) with coordinates $\mathbf{r} = (x, y)^T$ and gradient operator $\nabla = (\partial/\partial x, \partial/\partial y)^T$. As explained in more detail in Bücker et al. (2018), multiplying all coefficients in equations (A1) and (A2) by y yields a transformation to cylindrical coordinates.

A1. Static Solution

The static problem set up by equations (6) and (7) is implemented by setting $u_1 = U^{(0)}(\mathbf{r})$, $c_1 = y\epsilon_0\epsilon_a$, $f_1 = -y2C_{\pm}^{\infty} e \sinh(u_1 e/(kT))$ in the electrolyte as well as $c_1 = y\epsilon_0\epsilon_a$ and $f_1 = 0$ in the solid phase. Note that in this appendix, coefficients are assumed to be zero if not specified differently.

The fixed surface-charge boundary condition (15) is realized by setting $g = -y\Sigma_d^{(0)}$ on all charged boundaries. The definition of the zero reference potential, equation (14), depends on the specific model: In the grain geometry, we set $s = 0$ on the left, right, and top boundary; in the membrane geometry, we define the point-wise constraint $u_1 = 0$ at two positions $(x = \pm(L_1+L_2)/2, y = 0)$ located on the left and right boundary, respectively. In this case, standard no-flow boundary conditions are set on the remaining parts of left and right boundary, as well as on the uncharged parts of the top boundary. Because $y = 0$ is the symmetry axis (selecting rotational symmetry in the model setup), no specific boundary conditions are defined on this boundary.

A2. Frequency-Dependent Solution

For the frequency-dependent problem set up by the coupled PDEs (8) and (9), which describe the physics in the electrolyte, the Laplace equation (13), which controls the electrical field in the solid phase, and equation (11), which controls the surface charge in the Stern layer, need to be solved simultaneously. We use the same dependent variable u_2 in the electrolyte and in the solid phase and define suitable PDE coefficients on each of the two subdomains. The variable u_2 writes

$$\mathbf{u}_2 = \begin{bmatrix} u_{21} \\ u_{22} \\ u_{23} \end{bmatrix} = \begin{bmatrix} \delta C_-(\mathbf{r}, \omega) \\ \delta C_+(\mathbf{r}, \omega) \\ \delta U(\mathbf{r}, \omega) \end{bmatrix}. \tag{A4}$$

Assuming isotropic properties, the coefficient c_2 is a 3-by-3 coefficient matrix. In the electrolyte it writes

$$\underline{c}_2 = \begin{bmatrix} yD & 0 & -y\mu C_-^{\infty} \exp(\frac{e}{kT}u_1) \\ 0 & yD & y\mu C_+^{\infty} \exp(-\frac{e}{kT}u_1) \\ 0 & 0 & y\epsilon_0\epsilon_a \end{bmatrix}, \tag{A5}$$

and in the solid phase

$$\underline{c}_2 = \begin{bmatrix} 0 & 0 & 0 \\ 0 & 0 & 0 \\ 0 & 0 & y\epsilon_0\epsilon_i \end{bmatrix}. \tag{A6}$$

The variable u_1 is the static part of the electrical potential. The coefficient matrix $\underline{\alpha}$ writes

$$\underline{\alpha}_2 = \begin{bmatrix} -y\mu\nabla u_1 & 0 & 0 \\ 0 & y\mu\nabla u_1 & 0 \\ 0 & 0 & 0 \end{bmatrix} \tag{A7}$$

in the electrolyte and is equal to the null matrix in the solid phase. Note that on our two-dimensional modeling domain, each element of the matrix $\underline{\alpha}_2$ is a two-element vector. The matrix $\underline{a}_2$ is

$$\underline{a}_2 = \begin{bmatrix} yi\omega & 0 & 0 \\ 0 & yi\omega & 0 \\ yF & -yF & 0 \end{bmatrix} \tag{A8}$$

in the electrolyte. In the solid phase, $\underline{a}_2$ is the same except for the last line, which has to be filled with zeros instead.

Equation (11) describing the perturbation surface-charge density $\delta\Sigma_S$ is solved on the solid-liquid interface only. By means of a so-called lower-dimensional physics interface, the curvature of this interface is taken into account. Because the electrical potential in the Stern layer has to be equal to the potentials δU_i and δU_a on the corresponding boundaries, the only dependent variable on the interface is $u_3 = \delta\Sigma_S(\mathbf{r}_S, \omega)$. The coefficients are $c_3 = yD_S$, $a_3 = yi\omega$, and $\gamma_3 = -y\mu_S\Sigma_S^{(0)}\nabla u_{23}$, where u_{23} denotes the perturbation potentials on the adjacent two-dimensional subdomains.

The boundary condition (16) describing the external excitation and the condition on the perturbation concentrations (17) are realized by setting $\mathbf{s}_2 = (0, 0, \pm E_0 L)^T$. In the membrane-polarization model with the continuous EDL, this boundary is not located at a far distance from the charged surface. However, because of the symmetry of the problem with respect to $x = 0$, we expect the perturbation ion concentrations to vanish in this geometry, too (see, e.g., concentration profiles in Blaschek & Hördt, 2009). For the same reason, the perturbation surface-charge density $\delta\Sigma_S$ is also expected to vanish on the left and right boundary, and we set $s_3 = 0$ (only for a continuous EDL).

On the solid-liquid interface, we implement the zero-flux boundary conditions (19) and the condition on the displacement current (20) by defining $\mathbf{g} = (0, 0, yu_3)^T$.

On the top boundary, we implement zero-flux boundary condition on all three components of u_2 resulting in vanishing normal ion fluxes and a vanishing normal electrical field. In the membrane-polarization model with the continuous EDL, parts of the top boundary represent charged surfaces and are furnished with the corresponding boundary conditions described above. In the membrane-polarization model with the discontinuous EDL, the one-dimensional domain representing the Stern layer ends at the top boundary. In this case, we also define no-flux boundary conditions for u_3.

A3. Model Discretization

Special care has to be taken with the model discretization: While particle and pore sizes are in the micrometer to millimeter range, the thickness of the diffuse layer is orders of magnitude smaller. We use a special quadrangle boundary-layer mesh at the solid-liquid interface, which in radial direction consists of eight elements with sizes increasing from $\lambda_D/2$ at the surface to $\approx 1.8\lambda_D$ at the outer edge. In tangential direction (i.e., along the boundaries), the elements have a size of $\pi a/400$ in the grain-based model and $R_2/5$ in the pore-constriction geometry. The remaining volume is filled with triangular elements, the maximum size of which increases from $\pi a/400$ (or $R_2/5$) at the edge of the boundary-layer meshes to $L/20$ (or $R_1/5$) at the remote boundaries. For a spherical particle of radius $a = 5\,\mu\text{m}$, this results in a total of ≈20,900 elements, of which 6,400 elements correspond to the boundary-layer mesh. For pore lengths $L_1 = 90\,\mu\text{m}$ and $L_2 = 10$ μn and pore radii $R_1 = 2\,\mu\text{m}$ and $R_2 = 0.2\,\mu\text{m}$, the meshes consist of ≈14,700 elements (≈11,000 for the continuous EDL), of which ≈5,200 (≈7,600) elements make the boundary-layer mesh.

Acknowledgments

M. Bücker acknowledges the Austrian Federal Ministry of Science, Research and Economy (project Development of Geophysical Exploration Methods for the Characterization of Mine-Tailings Towards Exploitation) and the German Academic Exchange Service (DAAD) for scholarships received for his work on this study. All authors gratefully acknowledge P. Leroy and one anonymous reviewer for their insightful comments that helped to improve the manuscript. Scripts, numerical models, and data used for this manuscript are available at Zenodo (https://doi.org/10.5281/zenodo.3067277).

References

Atekwana, E. A., & Slater, L. D. (2009). Biogeophysics: A new frontier in earth science research. *Reviews of Geophysics*, *47*, RG4004. https://doi.org/10.1029/2009RG000285

Atkins, P., & De Paula, J. (2013). *Elements of Physical Chemistry*. USA: Oxford University Press.

Bairlein, K., Bücker, M., Hördt, A., & Hinze, B. (2016). Temperature dependence of spectral induced polarization data: experimental results and membrane polarization theory. *Geophysical Journal International*, *205*, 440–453.

Bikerman, J. (1933). Ionentheorie der Elektrosmose, der Strömungsströme und der Oberflächenleitfähigkeit. *Zeitschrift für Physikalische Chemie A*, *163*, 378–394.

Blaschek, R., & Hördt, A. (2009). Numerical modelling of the IP effect at the pore scale. *Near Surface Geophysics*, *7*(5-6), 579–588.

Börner, F., Schopper, J., & Weller, A. (1996). Evaluation of transport and storage properties in the soil and groundwater zone from induced polarization measurements. *Geophysical Prospecting*, *44*(4), 583–601.

Bruggeman, D. A. G. (1935). Berechnung verschiedener physikalischer Konstanten von heterogenen Substanzen. I. Dielektrizitätskonstanten und Leitfähigkeiten der Mischkörper aus isotropen Substanzen. *Annalen der Physik*, *416*(7), 636–664.

Buchheim, W., & Irmer, G. (1979). Zur Theorie der induzierten galvanischen Polarisation in Festkörpern mit elektrolytischer Porenfüllung. *Gerlands Beiträge zur Geophysik*, *88*, 53–72.

Bücker, M., Flores Orozco, A., Hördt, A., & Kemna, A. (2017). An analytical membrane-polarization model to predict the complex conductivity signature of immiscible liquid hydrocarbon contaminants. *Near Surface Geophysics*, *15*(6), 547–562.

Bücker, M., & Hördt, A. (2013a). Analytical modelling of membrane polarization with explicit parametrization of pore radii and the electrical double layer. *Geophysical Journal International*, *194*, 804–813.

Bücker, M., & Hördt, A. (2013b). Long and short narrow pore models for membrane polarization. *Geophysics*, *78*(6), E299–E314.

Bücker, M., Undorf, S., Flores Orozco, A., & Kemna, Andreas. (2018). Electro-chemical polarization around metallic particles-Part 2: The role of diffuse surface charge. *Geophysics*, *84*(2), 1–64.

Chew, W., & Sen, P. (1982a). Potential of a sphere in an ionic solution in thin double layer approximations. *The Journal of Chemical Physics*, *77*(4), 2042–2044.

Chew, W., & Sen, P. (1982b). Dielectric enhancement due to electrochemical double layer: Thin double layer approximation. *The Journal of Chemical Physics*, *77*(9), 4683–4693.

de Lima, O. A., & Sharma, M. M. (1992). A generalized Maxwell-Wagner theory for membrane polarization in shaly sands. *Geophysics*, *57*(3), 431–440.

DeLacey, E. H., & White, L. R. (1981). Dielectric response and conductivity of dilute suspensions of colloidal particles. *Journal of the Chemical Society, Faraday Transactions 2: Molecular and Chemical Physics*, *77*(11), 2007–2039.

Dukhin, S., & Shilov, V. (1974). *Dielectric phenomena and the double layer in disperse systems and polyelectrolytes*. New York: Wiley.

Fixman, M. (1980). Charged macromolecules in external fields. I. The sphere. *The Journal of Chemical Physics*, *72*(9), 5177–5186.

Flores Orozco, A., Williams, K. H., Long, P. E., Hubbard, S. S., & Kemna, A. (2011). Using complex resistivity imaging to infer biogeochemical processes associated with bioremediation of an uranium-contaminated aquifer. *Journal of Geophysical Research*, *116*, G03001. https://doi.org/10.1029/2010JG001591

Fridrikhsberg, D. A., & Sidorova, M. P. (1961). A study of relationship between the induced polarization phenomenon and the electro-kinetic properties of capillary systems (in Russian). *Vestnik Leningradskogo Universiteta, Seria Chimia*, *4*, 222–226.

Garcia, A., Grosse, C., & Brito, P. (1985). On the effect of volume charge distribution on the Maxwell-Wagner relaxation. *Journal of Physics D: Applied Physics*, *18*(4), 739.

Grahame, D. C. (1947). The electrical double layer and the theory of electrocapillarity. *Chemical Reviews*, *41*(3), 441–501.

Grosse, C., & Shilov, V. N. (1996). Theory of the low-frequency electrorotation of polystyrene particles in electrolyte solution. *The Journal of Physical Chemistry*, *100*(5), 1771–1778.

Hördt, A., Bairlein, K., Bielefeld, A., Bücker, M., Kuhn, E., Nordsiek, S., & Stebner, H. (2016). The dependence of induced polarization on fluid salinity and pH, studied with an extended model of membrane polarization. *Journal of Applied Geophysics*, *135*, 408–417.

Hanai, T. (1960). Theory of the dielectric dispersion due to the interfacial polarization and its application to emulsions. *Kolloid-Zeitschrift*, *171*(1), 23–31.

Hinch, E. J., Sherwood, J. D., Chew, W. C., & Sen, P. N. (1984). Dielectric response of a dilute suspension of spheres with thin double layers in an asymmetric electrolyte. *Journal of the Chemical Society, Faraday Transactions 2: Molecular and Chemical Physics*, *80*(5), 535–551.

Hördt, A., Druiventak, A., Blaschek, R., Binot, F., Kemna, A., Kreye, P., & Zisser, N. (2009). Case histories of hydraulic conductivity estimation with induced polarization at the field scale. *Near Surface Geophysics*, *7*(5-6), 529–545.

Hördt, A., Bairlein, K., Bücker, M., & Stebner, H. (2017). Geometrical constraints for membrane polarization. *Near Surface Geophysics*, *15*, 579–592.

Hunter, R. (1981). *Zeta potential in colloid science: Principles and applications*. London: Academic Press.

Kemna, A., Binley, A., Cassiani, G., Niederleithinger, E., Revil, A., Slater, L., et al. (2012). An overview of the spectral induced polarization method for near-surface applications. *Near Surface Geophysics*, *10*(6), 453–468.

Kijlstra, J., van Leeuwen, H. P., & Lyklema, J. (1992). Effects of surface conduction on the electrokinetic properties of colloids. *Journal of the Chemical Society, Faraday Transactions*, *88*(23), 3441–3449.

Kosmulski, M. (2006). Electric charge density of silica, alumina, and related surfaces. In P. Somasundaran (Ed.), *Encyclopedia of surface and colloid science* (Vol. *3*, pp. 1857–1867). New York, London: CRC press.

Leroy, P., Li, S., Jougnot, D., Revil, A., & Wu, Y. (2017). Modelling the evolution of complex conductivity during calcite precipitation on glass beads. *Geophysical Journal International*, *209*(1), 123–140.

Leroy, P., & Revil, A. (2004). A triple-layer model of the surface electrochemical properties of clay minerals. *Journal of Colloid and Interface Science*, *270*(2), 371–380.

Leroy, P., & Revil, A. (2009). A mechanistic model for the spectral induced polarization of clay materials. *Journal of Geophysical Research*, *114*, B10202. https://doi.org/10.1029/2008JB006114

Leroy, P., Revil, A., Kemna, A., Cosenza, P., & Ghorbani, A (2008). Complex conductivity of water-saturated packs of glass beads. *Journal of Colloid and Interface Science*, *321*(1), 103–117.

Lesmes, D. P., & Morgan, F. D. (2001). Dielectric spectroscopy of sedimentary rocks. *Journal of Geophysical Research*, *106*(B7), 13,329–13,346.

Lyklema, J., Dukhin, S., & Shilov, V. (1983). The relaxation of the double layer around colloidal particles and the low-frequency dielectric dispersion: Part I. Theoretical considerations. *Journal of Electroanalytical Chemistry and Interfacial Electrochemistry*, *143*(1-2), 1–21.

Marshall, D. J., & Madden, T. R. (1959). Induced polarization, a study of its causes. *Geophysics*, *24*(4), 790–816.

Maxwell, J. C. (1892). *A treatise on electricity and magnetism* (3rd ed.). Oxford, England: Clarendon.

O'Konski, C. T. (1960). Electric properties of macromolecules. V. Theory of ionic polarization in polyelectrolytes. *The Journal of Physical Chemistry*, *64*(5), 605–619.

Revil, A., Cathles, L., Losh, S., & Nunn, J. (1998). Electrical conductivity in shaly sands with geophysical applications. *Journal of Geophysical Research*, *103*(B10), 23,925–23,936.

Revil, A., & Florsch, N. (2010). Determination of permeability from spectral induced polarization in granular media. *Geophysical Journal International*, *181*(3), 1480–1498.

Revil, A., & Glover, P. W. J. (1997). Theory of ionic-surface electrical conduction in porous media. *Physical Review B*, *55*(3), 1757.

Revil, A., & Glover, P. W. J. (1998). Nature of surface electrical conductivity in natural sands, sandstones, and clays. *Geophysical Research Letters*, *25*(5), 691–694.

Robinson, D. A., & Friedman, S. P. (2003). A method for measuring the solid particle permittivity or electrical conductivity of rocks, sediments, and granular materials. *Journal of Geophysical Research*, *108*(B2), 2076. https://doi.org/10.1029/2001JB000691

Schmutz, M., Revil, A., Vaudelet, P., Batzle, M., Viñao, P. F., & Werkema, D. (2010). Influence of oil saturation upon spectral induced polarization of oil-bearing sands. *Geophysical Journal International*, *183*(1), 211–224.

Schurr, J. (1964). On the theory of the dielectric dispersion of spherical colloidal particles in electrolyte solution. *The Journal of Physical Chemistry*, *68*(9), 2407–2413.

Schwarz, G. (1962). A theory of the low-frequency dielectric dispersion of colloidal particles in electrolyte solution. *The Journal of Physical Chemistry*, *66*(12), 2636–2642.

Shilov, V. N., Delgado, A. V., Gonzalez-Caballero, F., & Grosse, C. (2001). Thin double layer theory of the wide-frequency range dielectric dispersion of suspensions of non-conducting spherical particles including surface conductivity of the stagnant layer. *Colloids and Surfaces A: Physicochemical and Engineering Aspects*, *192*(1), 253–265.

Somasundaran, P. (2006). *Encyclopedia of surface and colloid science* (Vol. 2). New York, London: CRC press.

Stebner, H., Halisch, M., & Hördt, A. (2017). Simulation of membrane polarization of porous media with impedance networks. *Near Surface Geophysics*, *15*, 563–578.

Titov, K., Kemna, A., Tarasov, A., & Vereecken, H. (2004). Induced polarization of unsaturated sands determined through time domain measurements. *Vadose Zone Journal*, *3*(4), 1160–1168.

Titov, K., Komarov, V., Tarasov, V., & Levitski, A. (2002). Theoretical and experimental study of time domain-induced polarization in water-saturated sands. *Journal of Applied Geophysics*, *50*(4), 417–433.

Volkmann, J., & Klitzsch, N. (2010). Frequency-dependent electric properties of microscale rock models for frequencies from one millihertz to ten kilohertz. *Vadose Zone Journal*, *9*(4), 858–870.

Wagner, KarlW. (1914). Erklärung der Dielektrischen Nachwirkungsvorgänge auf Grund Maxwellscher Vorstellungen. *Electrical Engineering (Archiv fur Elektrotechnik)*, *2*(9), 371–387.

Wainwright, H. M., Flores Orozco, A., Bücker, M., Dafflon, B., Chen, J., Hubbard, S. S., & Williams, K. H. (2015). Hierarchical Bayesian method for mapping biogeochemical hot spots using induced polarization imaging. *Water Resources Research*, *52*, 533–551. https://doi.org/10.1002/2015WR017763

Zukoski, C. F., & Saville, D. A. (1986). The interpretation of electrokinetic measurements using a dynamic model of the stern layer: II. Comparisons between theory and experiment. *Journal of colloid and interface science*, *114*(1), 45–53.